

Prospects for Distinguishing Supernova Models Using a Future Neutrino Signal

Jackson Olsen and Yong-Zhong Qian

School of Physics and Astronomy, University of Minnesota, Minneapolis, Minnesota 55455

(Dated: February 22, 2022)

The next Galactic core-collapse supernova (SN) should yield a large number of observed neutrinos. Using Bayesian techniques, we show that with an SN at a known distance up to 25 kpc, the neutrino events in a water Cherenkov detector similar to Super-Kamiokande (SK) could be used to distinguish between seven one-dimensional neutrino emission models assuming no flavor oscillations or the standard Mikheyev-Smirnov-Wolfenstein effect. Some of these models could still be differentiated with an SN at a known distance of 50 kpc. We also consider just the relative distributions of neutrino energy and arrival time predicted by the models and find that a detector like SK meets the requirement to distinguish between these distributions with an SN at an unknown distance up to ~ 10 kpc.

I. INTRODUCTION

Since the observation of Supernova 1987A (SN 1987A) and its associated neutrino signal, theoretical work on core-collapse SNe and their neutrino emission has advanced significantly (see, e.g., [1, 2] for recent reviews). Today, both one-dimensional (1D) and multi-D (2D and 3D) models of SN neutrino emission can be simulated beyond ~ 1 s (e.g., [2, 3]). In [4], we took the Bayesian approach to compare three 1D models provided by the Garching group [5] with the SN 1987A data from the Kamiokande II (KII) detector [6, 7]. While providing some discrimination among the models, the sparse KII data prevented us from drawing definitive conclusions. More useful will be a future neutrino signal from a Galactic SN, which is expected to result in a great many neutrino events in current and planned detectors (e.g., [8]). The actual number of events will depend on the distance to the SN, the details of the neutrino emission, and the detector of concern.

The authors of [9] performed a detailed study of the feasibility of distinguishing between five SN models using hypothetical neutrino data in the planned Hyper-Kamiokande (HK) detector (e.g., [10]). They focused on an early phase of neutrino emission spanning 500 ms, which is closely related to the explosion mechanism. Assuming that the distance to the SN is unknown, they studied the relative distributions of neutrino energy and arrival time predicted by the models. Taking into account flavor oscillations due to the Mikheyev-Smirnov-Wolfenstein (MSW) effect, they performed detailed reconstruction of 100 and 300 simulated events in the HK detector. In addition to the dominant inverse beta decay (IBD) reaction of $\bar{\nu}_e$ on protons, they also included scattering of all neutrino species on electrons and charged-current reactions of ν_e and $\bar{\nu}_e$ on ^{16}O . They concluded that all the five models could be distinguished with 300 events, which are expected from an SN at a distance of ~ 60 – 100 kpc for these models. A further analysis similar to the above was carried out in [11] to study the feasibility of distinguishing between four models that differ specifically in the mass or initial metallicity of the SN progenitor.

In this paper, we present a complementary study to those of [9, 11]. We focus on seven 1D SN models provided by the Garching group [5]. None of these models were considered in [9, 11]. Each model covers neutrino emission for at least 9 s, which allows us to explore the proto-neutron star (PNS) cooling phase in addition to the accretion phase of interest to [9, 11]. To cover the range of possible characteristics of water Cherenkov detectors, we consider both a detector similar to Super-Kamiokande (SK) and an idealized version. Following the treatments used extensively in the analyses of the SN 1987A neutrino data (e.g., [4, 12]), we consider only the dominant IBD detection channel. We allow for the Poisson statistics of the number of neutrino events and study the discriminating power of our assumed detectors for an SN at a specific distance. We analyze separately the cases where the distance to the SN is known or unknown. In addition to the MSW effect with the normal or inverted neutrino mass hierarchy considered in [9, 11], we also include the case of no oscillations for reference. We employ the Bayesian statistics to test the distinguishability of pairs of SN models for each of these three oscillation cases, and study the feasibility of distinguishing between these cases for a specific SN model. We find that all seven models can be distinguished from each other by an SK-like detector with an SN at a known distance up to at least 25 kpc or at an unknown distance up to at least ~ 10 kpc. In addition, provided that the underlying model is known, the three oscillation cases can be distinguished from each other with our assumed ideal detector and an SN at a known distance of 10 kpc.

The rest of the paper proceeds as follows. In Sec. II we describe the seven SN neutrino emission models and the two hypothetical detectors used in this work. In Sec. III we first perform a Monte Carlo study of the signal from one SN model and illustrate our general methodology of using the Bayes factor to distinguish a pair of models. We then present the mean Bayes factors and the associated standard deviations for various pairs of models assuming an SN at several known distances. In Sec. IV we calculate the combination of detector mass, detection efficiency, and SN distance required to distinguish between each pair of models assuming an unknown distance to the SN.

We summarize our results and give conclusions in Sec. V.

II. NEUTRINO EMISSION AND DETECTION

We employ seven models of SN neutrino emission in our analysis, all of which are 1D simulations provided by the Garching group [5]. They differ in the progenitor mass and the nuclear equation of state (EoS) used, and are designated as z9.6-LS220, z9.6-SFHo, s18.6-LS220, s18.6-SFHo, s20-SFHo, s27-LS220, and s27-SFHo. The z9.6, s18.6, s20, and s27 models correspond to progenitor masses of 9.6, 18.6, 20, and 27 M_\odot , respectively. The designation LS220 or SFHo corresponds to the EoS of [13] or [14], respectively. To keep our analysis consistent across the models, we use 9 s of neutrino emission. Some of these models were described in detail in [2].

The progenitor mass mainly influences the accretion phase of neutrino emission, during which matter falls onto the PNS before shock revival, releasing primarily ν_e and $\bar{\nu}_e$. The density of the infalling matter depends on the progenitor structure. The slower decrease of density with radius for more massive progenitors delays the shock revival to later times, and therefore, leads to a longer accretion phase (up to ~ 0.6 s for s20 and s27 models). The EoS mainly influences the emission due to cooling of the PNS, which lasts $\gtrsim 10$ s. For convenience, we refer to the period after the accretion phase as the PNS cooling phase, although PNS cooling starts at the same time as accretion-induced emission. In contrast to the accretion phase with dominant emission of ν_e and $\bar{\nu}_e$, the PNS cooling phase is characterized by approximately equal luminosities for ν_e , $\bar{\nu}_e$, ν_x , and $\bar{\nu}_x$ ($x = \mu$ or τ).

Figure 1 shows the characteristics of $\bar{\nu}_e$ and $\bar{\nu}_x$ emission as functions of time for our adopted models. The evolution of $\bar{\nu}_e$ and $\bar{\nu}_x$ luminosities, $L_{\bar{\nu}_e}$ and $L_{\bar{\nu}_x}$, is shown in the first row. The z9.6 models, with their low progenitor mass, have a very short accretion phase with only a little excess emission of $\bar{\nu}_e$ over $\bar{\nu}_x$. Differences between $L_{\bar{\nu}_e}$ and $L_{\bar{\nu}_x}$ for the s18.6 models indicate an accretion phase of moderate duration and intensity, while the pronounced differences for the s20 and s27 models reveal long and intense accretion-induced emission of $\bar{\nu}_e$. For all seven models, we see only small differences between $L_{\bar{\nu}_e}$ and $L_{\bar{\nu}_x}$ during the PNS cooling phase. The second row of Fig. 1 shows the evolution of the average $\bar{\nu}_e$ and $\bar{\nu}_x$ energies, $\langle E_{\bar{\nu}_e} \rangle$ and $\langle E_{\bar{\nu}_x} \rangle$. We see that $\langle E_{\bar{\nu}_x} \rangle$ is larger than $\langle E_{\bar{\nu}_e} \rangle$ initially, but the difference subsides after several seconds. We also see that the LS220 and SFHo models differ in that the former have a quicker drop of $\langle E_{\bar{\nu}_e} \rangle$ and $\langle E_{\bar{\nu}_x} \rangle$ during the PNS cooling phase. The third row of Fig. 1 shows the evolution of the spectral parameter

$$\alpha_\nu = \frac{2\langle E_\nu \rangle^2 - \langle E_\nu^2 \rangle}{\langle E_\nu^2 \rangle - \langle E_\nu \rangle^2} \quad (1)$$

for $\bar{\nu}_e$ and $\bar{\nu}_x$, where $\langle E_\nu^2 \rangle$ is the second moment of the neutrino energy spectrum. We see that $\alpha_{\bar{\nu}_e}$ and $\alpha_{\bar{\nu}_x}$ differ significantly at early times, but grow more similar at late

times. The difference between $\alpha_{\bar{\nu}_e}$ and $\alpha_{\bar{\nu}_x}$ is insensitive to the EoS at early times, but shows some dependence on the EoS at late times.

In the absence of neutrino oscillations, the energy-differential number flux of a neutrino species ν_β at a distance d to the SN is

$$F_{\nu_\beta}(E_\nu, t) = \frac{L_{\nu_\beta}}{4\pi d^2 \langle E_{\nu_\beta} \rangle} f_{\nu_\beta}(E_\nu, t), \quad (2)$$

where

$$f_{\nu_\beta}(E_\nu, t) = \frac{T_{\nu_\beta}^{-1}(t)}{\Gamma(1 + \alpha_{\nu_\beta}(t))} \left(\frac{E_\nu}{T_{\nu_\beta}(t)} \right)^{\alpha_{\nu_\beta}(t)} e^{-E_\nu/T_{\nu_\beta}(t)}, \quad (3)$$

with $\Gamma(1 + \alpha_{\nu_\beta})$ being the Gamma function and

$$T_{\nu_\beta} = \frac{\langle E_{\nu_\beta} \rangle}{1 + \alpha_{\nu_\beta}}, \quad (4)$$

is the normalized ν_β energy spectrum [15]. Note that although L_{ν_β} , $\langle E_{\nu_\beta} \rangle$, α_{ν_β} , and T_{ν_β} are functions of time, we often suppress their time dependence for convenience. Here and below, we use the emission time as the effective arrival time because the time of travel over a fixed distance only introduces a constant shift.

Because the IBD detection channel, $\bar{\nu}_e + p \rightarrow n + e^+$, has a cross section much larger than that of any other channel at the relevant neutrino energies [8, 16, 17], it will yield the highest number of SN neutrino events in water Cherenkov detectors. Most, if not all, of the neutrino events from SN 1987A were observed via this channel in such detectors [7, 8, 18]. With the recent addition of gadolinium in the detector, SK should have the capability of tagging the IBD events from a future SN [19]. Based on the above, we restrict our analysis in this paper to the IBD events in water Cherenkov detectors.

The expected energy-differential rate of IBD events including both the signal and the background is

$$\frac{d^2 N}{dt dE}(E, t) = B(E) + N_p \int F_{\text{det}}(E_\nu, t) \sigma_{\text{IBD}}(E_\nu) \times \frac{\epsilon(E_e)}{\sigma_E \sqrt{2\pi}} \exp\left[-\frac{(E - E_e)^2}{2\sigma_E^2}\right] dE_\nu, \quad (5)$$

where $B(E)$ is the background rate at energy E , N_p is the total number of free protons within the fiducial volume, $F_{\text{det}}(E_\nu, t)$ is the $\bar{\nu}_e$ flux at the detector, $\sigma_{\text{IBD}}(E_\nu)$ is the IBD cross section, $E_e = E_\nu - \Delta$ is the energy of the e^+ from the IBD reaction, $\Delta = 1.293$ MeV is the neutron-proton mass difference, and $\epsilon(E_e)$ is the detection efficiency. Because of smearing, an e^+ of energy E_e may be detected at energy E , the probability of which is approximated by a Gaussian distribution with an E_e -dependent standard deviation σ_E .

The flux $F_{\text{det}}(E_\nu, t)$ is affected by neutrino oscillations and is given by

$$F_{\text{det}}(E_\nu, t) = f F_{\bar{\nu}_e}(E_\nu, t) + (1 - f) F_{\bar{\nu}_x}(E_\nu, t), \quad (6)$$

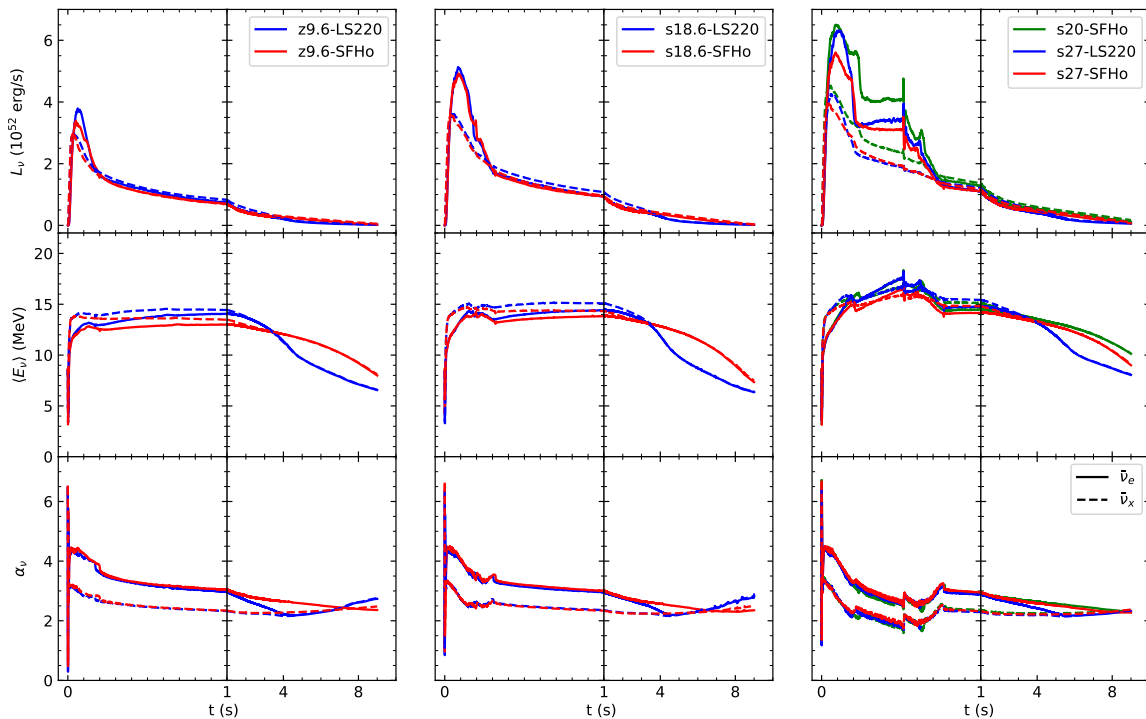


FIG. 1. The luminosity L_ν , average energy $\langle E_\nu \rangle$, and spectral parameter α_ν for $\bar{\nu}_e$ and $\bar{\nu}_x$ are displayed as functions of time for the adopted SN neutrino emission models. Note that the time scale changes at $t = 1$ s.

where the constant f specifies the degree of mixing between $\bar{\nu}_e$ and $\bar{\nu}_x$. We consider three cases of neutrino oscillations. The reference case NO with no oscillations corresponds to $f = 1$. The other two cases correspond to $f = 0.681$ or 0.022 for just the MSW effect with the normal (NH) or inverted (IH) neutrino mass hierarchy, respectively [20–22]. We add (NO), (NH), or (IH) to the label of a model to specify the assumed case of neutrino oscillations.

For a specific emission model M_α , the probability distribution for an event to be observed at time t with energy E is

$$p(E, t|M_\alpha) = \frac{1}{\langle N \rangle} \frac{d^2 N}{dt dE}, \quad (7)$$

where

$$\langle N \rangle = \int_0^{9 \text{ s}} dt \int_{E_{\min}}^{\infty} dE \frac{d^2 N}{dt dE} \quad (8)$$

is the expected total number of events and E_{\min} is the minimum energy for detection.

In the above discussion of SN neutrino detection, the quantities $B(E)$, N_p , $\epsilon(E_e)$, σ_E , and E_{\min} depend on the detector. We consider two hypothetical detectors to cover

a range of capabilities. One detector has a constant detection efficiency $\epsilon = 0.75$ and no background [$B(E) = 0$] when a minimum detected energy $E_{\min} = 7.5$ MeV is imposed. Its energy resolution is specified by the standard deviation σ_E for the smearing of the e^+ energy as

$$\frac{\sigma_E}{\text{MeV}} = -0.0839 + 0.349 \sqrt{\frac{E_e}{\text{MeV}}} + 0.0397 \left(\frac{E_e}{\text{MeV}} \right). \quad (9)$$

Because these characteristics are similar to those of SK (e.g., [23]), we refer to the above detector as the SK-like detector. We also consider an ideal detector that has no background [$B(E) = 0$] and can detect any e^+ above the threshold for Cherenkov radiation ($E_{\min} = 0.8$ MeV) with perfect detection efficiency ($\epsilon = 1$) and energy resolution [$\sigma_E = 0$, for which the Gaussian distribution becomes $\delta(E - E_e)$].

For both our hypothetical detectors, the event rate in Eq. (5) can be rewritten as

$$\begin{aligned} \frac{d^2 N}{dt dE}(E, t) &= A \int \tilde{F}_{\text{det}}(E_\nu, t) \sigma_{\text{IBD}}(E_\nu) \\ &\times \frac{1}{\sigma_E \sqrt{2\pi}} \exp \left[-\frac{(E - E_e)^2}{2\sigma_E^2} \right] dE_\nu, \end{aligned} \quad (10)$$

where $\tilde{F}_{\text{det}}(E_\nu, t) = F_{\text{det}}(E_\nu, t)/(d/\text{kpc})^2$ is the detected

TABLE I. Expected numbers of IBD events $\langle N \rangle$ in our SK-like and ideal detectors from an SN at a distance of 10 kpc for adopted SN models and assumed cases of neutrino oscillations.

Model	$\langle N \rangle$ (SK-like)	$\langle N \rangle$ (Ideal)
z9.6-LS220		
(NO)	2502.54	3553.15
(NH)	2651.36	3755.53
(IH)	2958.80	4173.62
z9.6-SFHo		
(NO)	2522.06	3611.22
(NH)	2645.24	3777.23
(IH)	2899.72	4120.17
s18.6-LS220		
(NO)	3517.01	4956.11
(NH)	3716.93	5222.31
(IH)	4129.93	5772.23
s18.6-SFHo		
(NO)	3763.67	5312.96
(NH)	3911.38	5511.05
(IH)	4216.54	5920.27
s20-SFHo		
(NO)	7152.88	9938.71
(NH)	7098.49	9863.93
(IH)	6986.13	9709.45
s27-LS220		
(NO)	5529.75	7693.13
(NH)	5503.49	7655.92
(IH)	5449.24	7579.06
s27-SFHo		
(NO)	5574.73	7786.92
(NH)	5608.19	7829.64
(IH)	5677.30	7917.90

flux from an SN at a distance of 1 kpc,

$$A = \epsilon N_p \left(\frac{\text{kpc}}{d} \right)^2 = 2.14 \times 10^{33} \epsilon \left(\frac{M_{\text{H}_2\text{O}}}{32 \text{ kton}} \right) \left(\frac{\text{kpc}}{d} \right)^2, \quad (11)$$

and $M_{\text{H}_2\text{O}}$ is the fiducial mass of water in the detector. We take $M_{\text{H}_2\text{O}} = 32 \text{ kton}$ (appropriate for SK [8]) for our calculations. The expected total numbers of events $\langle N \rangle$ in our hypothetical detectors from an SN at a distance of 10 kpc are given in Table I for our adopted SN models and assumed cases of neutrino oscillations. We note that here and below, our results also apply to other combinations of ϵ , $M_{\text{H}_2\text{O}}$, and d so long as they give the same values of A corresponding to our results.

III. ANALYSIS FOR KNOWN SN DISTANCE

We now present a Bayesian approach to test the distinguishability of our adopted SN models with an SN at a known distance. We first perform a Monte Carlo study of the signal from one model and illustrate our general methodology of using the Bayes factor to distinguish a pair of models. We then present the mean Bayes factors and the associated standard deviations for various pairs

of models assuming an SN at several known distances.

A. An Example

As a demonstration of our Bayesian approach, we consider the following example. We assume that an SN occurs at $d = 50 \text{ kpc}$ (approximately the distance of SN 1987A [24, 25]) with its neutrino emission described by the model z9.6-LS220(NO). To test how well we can distinguish between this true model and any other model, we generate a Monte Carlo sample of 10^4 instances of the signal in our assumed ideal detector from the above SN. For each simulated signal, we first pick the total number of events N from a Poisson distribution with an expected total number of events $\langle N \rangle = 142.13$ (see the corresponding entry for $d = 10 \text{ kpc}$ in Table I), and then draw N events from the distribution $p(E, t | \text{z9.6-LS220(NO)})$ [see Eq. (7)] to form a set $\{E_i, t_i | i = 1, 2, \dots, N\}$, where E_i and t_i are the energy and emission time of the i th event. Finally, for practical purposes, we define the detection time for the i th event as $t_{\text{det},i} = t_i - t_1$ so that the first detected event corresponds to $t_{\text{det}} = 0$. We denote each simulated signal by the data set $D = \{E_i, t_{\text{det},i} | i = 1, 2, \dots, N\}$.

Clearly, to compare a specific model M_α with the data, we need to introduce a time offset t_{off} between $t = 0$ for the start of neutrino emission in the model and $t_{\text{det}} = 0$ for detection of the first event so that $t = t_{\text{det}} + t_{\text{off}}$ (e.g., [4, 12]; the time of travel from the SN to the detector is the same for all the events, and therefore, can be ignored). The Bayesian approach to model comparison dictates that for M_α and the data D , the relevant quantity is the Bayesian evidence

$$P(D|M_\alpha) = \int dt_{\text{off}} P(D|t_{\text{off}}, M_\alpha) P(t_{\text{off}}), \quad (12)$$

where $P(D|t_{\text{off}}, M_\alpha)$ is the likelihood function assuming M_α , and $P(t_{\text{off}})$ is the prior probability for t_{off} . We take the likelihood of a simulated signal to be

$$P(D|t_{\text{off}}, M_\alpha) = \frac{e^{-\langle N \rangle} \langle N \rangle^N}{N!} \prod_{i=1}^N p(E_i, t_i | t_{\text{off}}, M_\alpha), \quad (13)$$

which follows from the extended maximum likelihood function of [26]. We take the prior $P(t_{\text{off}})$ to be uniform over the range $(0, 0.1 \text{ s})$ and 0 otherwise.

The Bayes factor

$$B_{\alpha\beta} = \frac{P(D|M_\alpha)}{P(D|M_\beta)} \quad (14)$$

can be used to determine whether M_α is favored over M_β given the data D . For convenience, we use the natural logarithm of the Bayes factor, $\ln B_{\alpha\beta}$, and refer to it simply as the Bayes factor. The criteria for interpreting $\ln B_{\alpha\beta}$ are shown in Table II (e.g., [12]). The larger $\ln B_{\alpha\beta}$ is, the more strongly M_α is favored over M_β .

TABLE II. Interpretation of the Bayes factor $\ln B_{\alpha\beta}$ (partially reproduced from [12]).

$\ln B_{\alpha\beta}$	Strength of Evidence
0–1	Not worth more than a bare mention
1–3	Positive
3–5	Strong
> 5	Very strong

TABLE III. The mean Bayes factors along with standard deviations $\langle \ln B_{\alpha\beta} \rangle \pm \sigma[\ln B_{\alpha\beta}]$ calculated with M_α being z9.6-LS220(NO) using 10^4 simulated signals in the assumed ideal detector from an SN at $d = 50$ kpc. The true model M_α can be distinguished from the alternative M_β at the $> 95\%$ CL for $\langle \ln B_{\alpha\beta} \rangle - 1.645\sigma[\ln B_{\alpha\beta}] > 5$, which is satisfied by all the entries except for those in bold.

M_β	Unknown t_{off}	$t_{\text{off}} = t_1$
z9.6-SFHo(NO)	9.52 ± 3.81	9.55 ± 3.81
s18.6-LS220(NO)	10.61 ± 4.17	10.80 ± 4.21
s18.6-SFHo(NO)	21.81 ± 5.32	21.97 ± 5.35
s20-SFHo(NO)	132.98 ± 11.54	133.42 ± 11.56
s27-LS220(NO)	70.14 ± 9.12	70.68 ± 9.15
s27-SFHo(NO)	74.50 ± 9.18	74.82 ± 9.20

We calculate the Bayesian evidence for each of our models, and compute the Bayes factors with M_α and M_β being z9.6-LS220(NO) and each of the corresponding alternative models, respectively. Performing this procedure for the 10^4 simulated signals in our Monte Carlo sample allows us to calculate the mean $\langle \ln B_{\alpha\beta} \rangle$ and standard deviation $\sigma[\ln B_{\alpha\beta}]$ for the six model pairs. The results are displayed in the second column of Table III. We see that for each alternative model, $\langle \ln B_{\alpha\beta} \rangle > 5$, which indicates that at $d = 50$ kpc with an ideal detector, a neutrino signal following z9.6-LS220(NO) would on average provide very strong evidence in favor of the true model over the corresponding alternatives.

We can set an even more stringent criterion for model distinguishability by noting that the distribution of $\ln B_{\alpha\beta}$ is approximately normal as demonstrated in Fig. 2 with M_α and M_β being z9.6-LS220(NO) and z9.6-SFHo(NO), respectively. The histogram in Fig. 2 shows the binned results for the Monte Carlo sample, which are very well described by the curve for the normal distribution with the corresponding $\langle \ln B_{\alpha\beta} \rangle$ and $\sigma[\ln B_{\alpha\beta}]$. We consider that the true model M_α can be distinguished from the alternative M_β for $\ln B_{\alpha\beta} > 5$. We say that M_α and M_β are distinguishable at the $> 95\%$ confidence level (CL) if $\langle \ln B_{\alpha\beta} \rangle - 1.645\sigma[\ln B_{\alpha\beta}] > 5$. From the $\langle \ln B_{\alpha\beta} \rangle$ and $\sigma[\ln B_{\alpha\beta}]$ values in the second column of Table III, we see that at $d = 50$ kpc with an ideal detector, a neutrino signal following z9.6-LS220(NO) can be distinguished at the $> 95\%$ CL from all the other adopted models except for z9.6-SFHo(NO) (see also Fig. 2) and s18.6-LS220(NO).

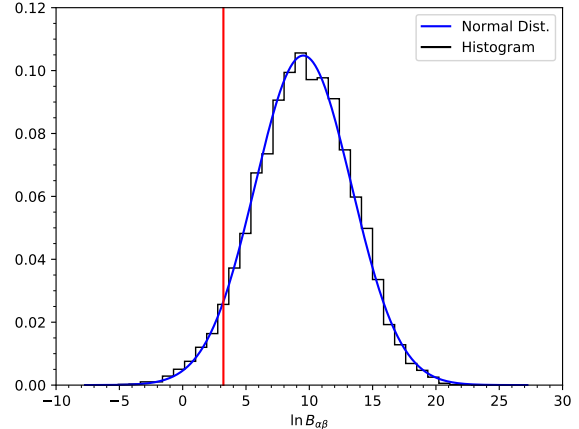


FIG. 2. The histogram of $\ln B_{\alpha\beta}$ is compared to the curve for the corresponding normal distribution with M_α and M_β being z9.6-LS220(NO) and z9.6-SFHo(NO), respectively. The vertical line corresponds to $\ln B_{\alpha\beta} = \langle \ln B_{\alpha\beta} \rangle - 1.645\sigma[\ln B_{\alpha\beta}]$, and 95% of the $\ln B_{\alpha\beta}$ values lie to the right of this line. These results are based on 10^4 simulated signals in the assumed ideal detector from an SN at $d = 50$ kpc. An unknown time offset t_{off} between the start of neutrino emission and detection of the first event is taken into account.

B. General Results

While the procedure in Sec. III A for comparing M_α and M_β is straightforward, it can be simplified by setting $t_{\text{off}} = t_1$, where t_1 is the emission time of the first event for each simulated signal of M_α . With this simplification, we are directly comparing the distributions of neutrino energy and emission time for M_α and M_β by ignoring the effects of the time offset t_{off} between the start of emission and detection of the first event, and the Bayesian evidence for M_β is simply

$$P(D|M_\beta) = \frac{e^{-\langle N \rangle} \langle N \rangle^N}{N!} \prod_{i=1}^N p(E_i, t_i|M_\beta), \quad (15)$$

where $\{E_i, t_i | i = 1, 2, \dots, N\}$ effectively denotes a simulated signal of M_α . Using the 10^4 simulated signals of z9.6-LS220(NO) (M_α) in Sec. III A and setting $t_{\text{off}} = t_1$, we calculate the $\langle \ln B_{\alpha\beta} \rangle$ and $\sigma[\ln B_{\alpha\beta}]$ values for comparing this model with all the corresponding alternatives. As can be seen from Table III, these results are approximately the same as those that have taken the effects of t_{off} into account. Therefore, we can ignore the very small effects of t_{off} in calculating $\langle \ln B_{\alpha\beta} \rangle$ and $\sigma[\ln B_{\alpha\beta}]$ to determine the distinguishability of M_α and M_β .

Below we compare all pairs of our adopted models using the simplified procedure that does not include t_{off} as a parameter. The corresponding Bayes factor is

$$\ln B_{\alpha\beta} = N \ln \frac{\langle N \rangle_\alpha}{\langle N \rangle_\beta} - \Delta_{\alpha\beta} + \sum_{i=1}^N \ln \frac{p(E_i, t_i|M_\alpha)}{p(E_i, t_i|M_\beta)}, \quad (16)$$

where $\langle N \rangle_\alpha$ and $\langle N \rangle_\beta$ are the expected total numbers of events predicted by M_α and M_β , respectively, for an SN at a known distance d , and $\Delta_{\alpha\beta} \equiv \langle N \rangle_\alpha - \langle N \rangle_\beta$. With simulated neutrino signals from M_α , N is sampled from the Poisson distribution with the mean $\langle N \rangle_\alpha$, and $\{E_i, t_i | i = 1, 2, \dots, N\}$ is sampled from the energy-time distribution $\prod_{j=1}^N p(E_j, t_j | M_\alpha)$. Instead of Monte Carlo simulations, we can use the above distributions directly to obtain

$$\frac{\langle \ln B_{\alpha\beta} \rangle}{\langle N \rangle_\alpha} = \ln \frac{\langle N \rangle_\alpha}{\langle N \rangle_\beta} - \frac{\Delta_{\alpha\beta}}{\langle N \rangle_\alpha} + \left\langle \ln \frac{p(E, t | M_\alpha)}{p(E, t | M_\beta)} \right\rangle_\alpha \quad (17)$$

and

$$\begin{aligned} \frac{\sigma[\ln B_{\alpha\beta}]}{\sqrt{\langle N \rangle_\alpha}} = & \left[\left(\ln \frac{\langle N \rangle_\alpha}{\langle N \rangle_\beta} \right)^2 \right. \\ & + 2 \ln \frac{\langle N \rangle_\alpha}{\langle N \rangle_\beta} \left\langle \ln \frac{p(E, t | M_\alpha)}{p(E, t | M_\beta)} \right\rangle_\alpha \\ & \left. + \left\langle \left(\ln \frac{p(E, t | M_\alpha)}{p(E, t | M_\beta)} \right)^2 \right\rangle_\alpha \right]^{1/2}, \quad (18) \end{aligned}$$

where, for example,

$$\begin{aligned} \left\langle \ln \frac{p(E, t | M_\alpha)}{p(E, t | M_\beta)} \right\rangle_\alpha = & \int_0^{9 \text{ s}} dt \int_{E_{\min}}^\infty dE p(E, t | M_\alpha) \\ & \times \ln \frac{p(E, t | M_\alpha)}{p(E, t | M_\beta)}. \quad (19) \end{aligned}$$

Both $\langle \ln B_{\alpha\beta} \rangle$ and $\sigma[\ln B_{\alpha\beta}]$ are functions of the SN distance d and depend on the assumed detector.

The $\langle \ln B_{\alpha\beta} \rangle$ and $\sigma[\ln B_{\alpha\beta}]$ values for all pairs of the adopted SN neutrino emission models are given for an SN at $d = 50$ (25) kpc in Tables IV and V (VI and VII) for the assumed ideal and SK-like detectors, respectively. We see that, for either detector, all of the models can be distinguished from one another at the $> 95\%$ CL (with $\langle \ln B_{\alpha\beta} \rangle - 1.645\sigma[\ln B_{\alpha\beta}] > 5$) for $d = 25$ kpc, and some of the models can still be distinguished at the same CL for $d = 50$ kpc. Note that the results for comparing z9.6-LS220(NO) (M_α) with the corresponding alternatives in Table IV are in excellent agreement with those in Table III calculated with Monte Carlo simulations.

C. Scenarios of Neutrino Oscillations

So far we have assumed that the scenario of neutrino oscillations would be known and whichever it is, it applies to all SN neutrino emission models in the same way. It is interesting to note that the distinguishability of these models depends on the scenario of neutrino oscillations. For example, for an SN at $d = 50$ kpc with the assumed ideal detector, we can distinguish z9.6-LS220(IH) and z9.6-SFHo(IH) at the $> 95\%$ CL, but cannot do the same for z9.6-LS220(NH) and z9.6-SFHo(NH) (see Table IV).

We now explore the feasibility of distinguishing between the scenarios of neutrino oscillations for a specific underlying SN neutrino emission model. We again perform the comparisons using Eqs. (17) and (18). With more significant differences between $\bar{\nu}_e$ and $\bar{\nu}_x$ emission during the accretion phase, we expect that more pronounced accretion-induced emission allows for easier distinguishability of the oscillation scenarios. Because z9.6-LS220 and s20-SFHo represent the opposite extremes of accretion-induced neutrino emission (see Fig. 1), we focus on these two models. The results for an SN at $d = 50$, 25, and 10 kpc with the assumed ideal detector are presented in Tables VIII and IX. We see that at $d = 50$ kpc, only the (NO) and (IH) scenarios can be distinguished at the $> 95\%$ CL for s20-SFHo, but none of the scenarios can be distinguished for z9.6-LS220. At $d = 25$ kpc, only the (NO) and (NH) scenarios cannot be distinguished for s20-SFHo, while only the (NO) and (IH) scenarios can be distinguished for z9.6-LS220. Finally, at $d = 10$ kpc, all oscillation scenarios can be distinguished for either model.

IV. ANALYSIS FOR UNKNOWN SN DISTANCE

In Sec. III, assuming that the distance to the SN is known, we have computed the Bayesian evidence $P(D|M_\alpha)$ with a likelihood that accounts for both the energy-time distribution $p(E, t|M_\alpha)$ and the expected total number of events $\langle N \rangle_\alpha$ predicted by the SN neutrino emission model M_α . If the SN distance is not known, however, the expected total numbers of events effectively become parameters and it is practical to compare only the distributions $p(E, t|M_\alpha)$ and $p(E, t|M_\beta)$ to determine the distinguishability of M_α and M_β . In this case, it is more difficult to distinguish the models because the number of observed events can no longer be used to provide extra discriminating power.

For analysis of the case of unknown SN distance, we define

$$\langle N \rangle = A \langle n \rangle, \quad (20)$$

so that $\langle n \rangle$ contains all the dependence on the SN neutrino emission model [see Eq. (10)]. Note that A only depends on the actual but unknown SN distance and the characteristics of the assumed detector [see Eq. (11)].

The Bayesian evidence for M_β is now

$$P(D|M_\beta) = \prod_{i=1}^N p(E_i, t_i | M_\beta), \quad (21)$$

where $\{E_i, t_i | i = 1, 2, \dots, N\}$ denotes a signal of M_α . The Bayes factor for comparing M_α and M_β is

$$\ln B_{\alpha\beta} = \sum_{i=1}^N \ln \frac{p(E_i, t_i | M_\alpha)}{p(E_i, t_i | M_\beta)}. \quad (22)$$

TABLE IV. The mean Bayes factors along with standard deviations $\langle \ln B_{\alpha\beta} \rangle \pm \sigma[\ln B_{\alpha\beta}]$ calculated for the assumed ideal detector and an SN at $d = 50$ kpc. The true model M_α can be distinguished from the alternative M_β at the $> 95\%$ CL for $\langle \ln B_{\alpha\beta} \rangle - 1.645\sigma[\ln B_{\alpha\beta}] > 5$, which is satisfied by all the entries except for those in bold.

$M_\alpha \backslash M_\beta$	z9.6-LS220	z9.6-SFHo	s18.6-LS220	s18.6-SFHo	s20-SFHo	s27-LS220	s27-SFHo
z9.6-LS220							
(NO)		9.53 ± 3.86	10.78 ± 4.23	21.93 ± 5.37	133.28 ± 11.66	70.59 ± 9.24	74.73 ± 9.28
(NH)		10.75 ± 4.05	10.78 ± 4.28	22.01 ± 5.32	122.07 ± 11.34	60.77 ± 8.89	69.16 ± 8.97
(IH)		13.70 ± 4.52	11.41 ± 4.43	22.97 ± 5.29	104.54 ± 10.45	46.21 ± 8.01	61.74 ± 8.29
z9.6-SFHo							
(NO)	12.98 ± 6.07		25.58 ± 7.22	15.28 ± 4.97	125.61 ± 11.78	75.15 ± 9.18	67.69 ± 9.26
(NH)	15.00 ± 6.60		29.13 ± 7.85	14.86 ± 4.95	113.4 ± 11.61	65.89 ± 8.99	61.10 ± 9.07
(IH)	19.65 ± 7.66		37.53 ± 9.12	14.63 ± 4.96	92.84 ± 11.00	51.74 ± 8.41	50.82 ± 8.57
s18.6-LS220							
(NO)	13.01 ± 5.60	27.86 ± 8.08		11.93 ± 3.87	91.85 ± 9.75	38.85 ± 6.98	45.73 ± 7.14
(NH)	12.68 ± 5.46	30.75 ± 8.38		13.95 ± 4.20	82.57 ± 9.25	30.28 ± 6.40	42.12 ± 6.76
(IH)	13.23 ± 5.53	38.34 ± 9.27		18.62 ± 4.89	70.26 ± 8.12	19.57 ± 5.22	39.55 ± 6.12
s18.6-SFHo							
(NO)	33.59 ± 10.17	18.83 ± 6.81	19.23 ± 7.89		71.02 ± 9.32	37.30 ± 6.77	28.55 ± 6.24
(NH)	34.43 ± 10.41	17.88 ± 6.56	22.51 ± 8.56		60.49 ± 8.93	29.20 ± 6.37	23.16 ± 5.84
(IH)	37.58 ± 11.09	17.19 ± 6.37	29.87 ± 9.89		44.02 ± 7.95	18.30 ± 5.50	15.71 ± 5.01
s20-SFHo							
(NO)	258.83 ± 31.60	225.48 ± 28.40	180.31 ± 26.75	117.55 ± 19.80		34.63 ± 10.12	15.68 ± 6.08
(NH)	232.91 ± 29.89	187.49 ± 24.74	164.28 ± 25.83	92.27 ± 16.80		36.36 ± 10.47	13.45 ± 5.58
(IH)	206.21 ± 28.78	140.18 ± 20.47	153.87 ± 26.04	62.25 ± 13.34		40.68 ± 11.24	9.85 ± 4.72
s27-LS220							
(NO)	115.89 ± 19.44	134.20 ± 21.90	61.80 ± 14.00	61.91 ± 14.40	23.44 ± 5.65		11.08 ± 4.30
(NH)	92.48 ± 16.70	106.55 ± 18.50	44.63 ± 11.45	42.89 ± 11.28	24.10 ± 5.66		11.26 ± 4.22
(IH)	66.25 ± 13.76	75.20 ± 14.75	28.29 ± 9.06	22.89 ± 7.63	26.01 ± 5.76		12.64 ± 4.32
s27-SFHo							
(NO)	129.99 ± 21.28	106.66 ± 18.34	82.91 ± 17.41	42.30 ± 11.23	13.35 ± 4.77	13.78 ± 5.94	
(NH)	120.53 ± 20.60	89.85 ± 16.20	79.10 ± 17.32	31.64 ± 9.30	11.64 ± 4.49	14.66 ± 6.24	
(IH)	113.79 ± 20.60	69.67 ± 13.77	82.27 ± 18.34	20.01 ± 7.13	8.73 ± 3.94	17.39 ± 6.95	

Using the Poisson distribution of N with the mean $\langle N \rangle_\alpha$ and the energy-time distribution $\prod_{j=1}^N p(E_j, t_j | M_\alpha)$ for $\{E_i, t_i | i = 1, 2, \dots, N\}$, we follow the same procedure as in Sec. III B to obtain

$$\frac{\langle \ln B_{\alpha\beta} \rangle}{A \langle n \rangle_\alpha} = \left\langle \ln \frac{p(E, t | M_\alpha)}{p(E, t | M_\beta)} \right\rangle_\alpha \quad (23)$$

and

$$\frac{\sigma[\ln B_{\alpha\beta}]}{\sqrt{A \langle n \rangle_\alpha}} = \sqrt{\left\langle \left(\ln \frac{p(E, t | M_\alpha)}{p(E, t | M_\beta)} \right)^2 \right\rangle_\alpha}. \quad (24)$$

Note that $\langle \ln B_{\alpha\beta} \rangle \propto A$ and $\sigma[\ln B_{\alpha\beta}] \propto \sqrt{A}$. We define A_{\min} as the value of A that satisfies

$$\langle \ln B_{\alpha\beta} \rangle - 1.645\sigma[\ln B_{\alpha\beta}] = 5. \quad (25)$$

To distinguish the true model M_α from the alternative M_β at the $> 95\%$ CL, we require $A > A_{\min}$. The above approach follows the framework of Bayes Factor Design Analysis (see, e.g., [27, 28]). We present the results on A_{\min} for the assumed ideal and SK-like detectors in Tables X and XI, respectively. These A_{\min} values all correspond to $\langle N \rangle > 50$. Monte Carlo testing suggests that

the effects of t_{off} are small for $\langle N \rangle > 50$, which justifies our ignoring these effects in calculating A_{\min} .

For an SN at $d = 10$ kpc, $A = 2.14 \times 10^{31}$ and 1.61×10^{31} for the assumed ideal and SK-like detectors, respectively. Either value exceeds all the corresponding A_{\min} values in Table X or XI. Therefore, all of the energy-time distributions for the adopted SN neutrino emission models can be distinguished from each other at the $> 95\%$ CL with the signal in either detector from an SN at $d = 10$ kpc. Noting that $A \propto d^{-2}$, we can estimate the maximum SN distance for which a pair of models can be distinguished. Take the SK-like detector for example. The highest required value of $A_{\min} = 8.26 \times 10^{30}$, necessary to distinguish the true model z9.6-LS220(IH) from the alternative s18.6-LS220(IH), means that these two models can be distinguished for an SN at a distance up to ~ 14 kpc. In contrast, the lowest value of $A_{\min} = 1.53 \times 10^{29}$, required to distinguish the true model s20-SFHo(NO) from the alternative z9.6-LS220(NO), means that these two models can be distinguished for an SN at a distance up to ~ 103 kpc.

TABLE V. The mean Bayes factors along with standard deviations $\langle \ln B_{\alpha\beta} \rangle \pm \sigma[\ln B_{\alpha\beta}]$ calculated for the assumed SK-like detector and an SN at $d = 50$ kpc. The true model M_α can be distinguished from the alternative M_β at the $> 95\%$ CL for $\langle \ln B_{\alpha\beta} \rangle - 1.645\sigma[\ln B_{\alpha\beta}] > 5$, which is satisfied by all the entries except for those in bold.

$M_\alpha \backslash M_\beta$	z9.6-LS220	z9.6-SFHo	s18.6-LS220	s18.6-SFHo	s20-SFHo	s27-LS220	s27-SFHo
z9.6-LS220							
(NO)		6.88 ± 3.27	7.88 ± 3.62	15.96 ± 4.58	97.83 ± 10.00	51.96 ± 7.94	54.73 ± 7.95
(NH)		7.80 ± 3.45	7.91 ± 3.66	16.04 ± 4.54	89.56 ± 9.72	44.71 ± 7.64	50.65 ± 7.68
(IH)		9.98 ± 3.86	8.42 ± 3.81	16.75 ± 4.52	76.54 ± 8.95	33.91 ± 6.88	45.16 ± 7.09
z9.6-SFHo							
(NO)	9.36 ± 5.14		18.71 ± 6.15	11.22 ± 4.26	92.54 ± 10.14	55.49 ± 7.93	49.82 ± 7.97
(NH)	10.85 ± 5.59		21.34 ± 6.69	10.94 ± 4.25	83.55 ± 9.98	48.69 ± 7.76	45.00 ± 7.80
(IH)	14.24 ± 6.49		27.49 ± 7.77	10.78 ± 4.26	68.33 ± 9.45	38.23 ± 7.25	37.41 ± 7.36
s18.6-LS220							
(NO)	9.50 ± 4.79	20.37 ± 6.89		8.72 ± 3.31	67.47 ± 8.37	28.60 ± 6.02	33.52 ± 6.13
(NH)	9.30 ± 4.67	22.56 ± 7.17		10.20 ± 3.59	60.55 ± 7.93	22.24 ± 5.50	30.83 ± 5.79
(IH)	9.75 ± 4.75	28.18 ± 7.94		13.61 ± 4.19	51.28 ± 6.94	14.23 ± 4.46	28.83 ± 5.23
s18.6-SFHo							
(NO)	24.37 ± 8.64	13.79 ± 5.82	13.95 ± 6.68		52.31 ± 8.02	27.51 ± 5.85	21.01 ± 5.37
(NH)	24.99 ± 8.84	13.13 ± 5.61	16.33 ± 7.25		44.53 ± 7.68	21.54 ± 5.49	17.03 ± 5.02
(IH)	27.27 ± 9.41	12.64 ± 5.46	21.66 ± 8.38		32.29 ± 6.82	13.44 ± 4.72	11.50 ± 4.29
s20-SFHo							
(NO)	188.41 ± 26.79	164.42 ± 24.08	130.95 ± 22.61	85.72 ± 16.79		25.25 ± 8.62	11.51 ± 5.20
(NH)	169.63 ± 25.35	137.31 ± 21.09	119.22 ± 21.82	67.5 ± 14.31		26.50 ± 8.92	9.88 ± 4.77
(IH)	149.66 ± 24.33	102.66 ± 17.46	111.11 ± 21.92	45.40 ± 11.35		29.63 ± 9.57	7.22 ± 4.04
s27-LS220							
(NO)	84.57 ± 16.52	97.67 ± 18.52	44.99 ± 11.87	45.01 ± 12.18	17.13 ± 4.83		8.05 ± 3.67
(NH)	67.67 ± 14.24	78.02 ± 15.75	32.54 ± 9.73	31.35 ± 9.59	17.61 ± 4.84		8.21 ± 3.60
(IH)	48.35 ± 11.71	55.14 ± 12.58	20.43 ± 7.67	16.68 ± 6.48	19.01 ± 4.92		9.24 ± 3.70
s27-SFHo							
(NO)	94.60 ± 18.06	77.85 ± 15.58	60.17 ± 14.72	30.85 ± 9.54	9.82 ± 4.10	10.02 ± 5.06	
(NH)	87.72 ± 17.48	65.85 ± 13.83	57.33 ± 14.63	23.15 ± 7.93	8.56 ± 3.86	10.67 ± 5.31	
(IH)	82.57 ± 17.44	51.07 ± 11.76	59.38 ± 15.46	14.58 ± 6.07	6.41 ± 3.37	12.67 ± 5.92	

V. DISCUSSION AND CONCLUSIONS

Using Bayesian techniques, we have studied the feasibility of distinguishing between seven 1D SN neutrino emission models with the IBD events in an ideal or SK-like detector. For each model, the standard MSW effect with the normal or inverted neutrino mass hierarchy is considered along with the reference scenario of no neutrino oscillations. We regard that the true model M_α can be distinguished from the alternative M_β at the $> 95\%$ CL when the mean Bayes factor and the associated standard deviation satisfy $\langle \ln B_{\alpha\beta} \rangle - 1.645\sigma[\ln B_{\alpha\beta}] > 5$. We have shown that for each of the three neutrino oscillation scenarios, all the models can be distinguished from each other with the signal in either the ideal or SK-like detector from an SN at a known distance up to 25 kpc (see Tables VI and VII). Some of the models could still be distinguished with an SN at a known distance of 50 kpc (see Tables IV and V). We have also explored the feasibility of distinguishing between the oscillation scenarios for a specific SN neutrino emission model. Provided that the emission model is known, for example, from observations of the SN progenitor, these scenarios can be distinguished from each other with the assumed ideal detector and an SN at a known distance of 10 kpc (see Tables VIII and

IX). Finally, we have compared just the relative distributions of neutrino energy and arrival time predicted by the models and found that the requirement to distinguish between these distributions can be satisfied by either the ideal or SK-like detector for an SN at an unknown distance up to ~ 10 kpc (see Tables X and XI).

Our study covers a limited number of 1D SN neutrino emission models, but can be extended to other 1D and multi-D models in a straightforward manner. Similarly, our study focusing on the IBD events in water Cherenkov detectors can be generalized to other types of neutrino detectors as well. In carrying out the present study and future ones of this kind, our goal is to estimate the potential of current and planned neutrino detectors to distinguish between various SN models. In the event of an actual SN, similar Bayesian techniques to those presented here can be used to rank various SN neutrino emission models as discussed in [4] for the case of SN 1987A. In addition, a p -value test can be performed to check if a model is incompatible with the data [4]. Based on the results presented here, it is very likely that the neutrino signal from the next Galactic SN would allow us to differentiate a wide range of models.

TABLE VI. The mean Bayes factors along with standard deviations $\langle \ln B_{\alpha\beta} \rangle \pm \sigma[\ln B_{\alpha\beta}]$ calculated for the assumed ideal detector and an SN at $d = 25$ kpc. The true model M_α can be distinguished from the alternative M_β at the $> 95\%$ CL for $\langle \ln B_{\alpha\beta} \rangle - 1.645\sigma[\ln B_{\alpha\beta}] > 5$, which is satisfied by all the entries.

$M_\alpha \backslash M_\beta$	z9.6-LS220	z9.6-SFHo	s18.6-LS220	s18.6-SFHo	s20-SFHo	s27-LS220	s27-SFHo
z9.6-LS220							
(NO)		38.13 ± 7.72	43.14 ± 8.46	87.74 ± 10.75	533.14 ± 23.32	282.38 ± 18.47	298.91 ± 18.55
(NH)		42.99 ± 8.10	43.12 ± 8.56	88.05 ± 10.64	488.30 ± 22.68	243.07 ± 17.77	276.64 ± 17.94
(IH)		54.82 ± 9.03	45.64 ± 8.86	91.88 ± 10.57	418.17 ± 20.91	184.85 ± 16.02	246.98 ± 16.58
z9.6-SFHo							
(NO)	51.94 ± 12.15		102.30 ± 14.44	61.11 ± 9.94	502.43 ± 23.56	300.59 ± 18.36	270.75 ± 18.53
(NH)	60.00 ± 13.20		116.54 ± 15.70	59.46 ± 9.90	453.60 ± 23.22	263.55 ± 17.98	244.40 ± 18.15
(IH)	78.61 ± 15.32		150.13 ± 18.25	58.52 ± 9.91	371.34 ± 22.01	206.95 ± 16.82	203.28 ± 17.14
s18.6-LS220							
(NO)	52.03 ± 11.21	111.46 ± 16.15		47.7 ± 7.74	367.40 ± 19.50	155.42 ± 13.96	182.91 ± 14.29
(NH)	50.7 ± 10.91	122.98 ± 16.75		55.82 ± 8.39	330.26 ± 18.50	121.12 ± 12.80	168.47 ± 13.51
(IH)	52.92 ± 11.06	153.37 ± 18.54		74.47 ± 9.79	281.05 ± 16.24	78.28 ± 10.43	158.20 ± 12.24
s18.6-SFHo							
(NO)	134.35 ± 20.34	75.32 ± 13.62	76.94 ± 15.77		284.09 ± 18.64	149.18 ± 13.55	114.19 ± 12.48
(NH)	137.71 ± 20.81	71.52 ± 13.12	90.04 ± 17.12		241.96 ± 17.87	116.79 ± 12.74	92.65 ± 11.69
(IH)	150.33 ± 22.19	68.76 ± 12.75	119.47 ± 19.78		176.10 ± 15.91	73.20 ± 10.99	62.85 ± 10.01
s20-SFHo							
(NO)	1035.31 ± 63.20	901.91 ± 56.79	721.24 ± 53.50	470.21 ± 39.59		138.53 ± 20.25	62.73 ± 12.15
(NH)	931.65 ± 59.78	749.94 ± 49.49	657.10 ± 51.66	369.08 ± 33.59		145.45 ± 20.94	53.79 ± 11.15
(IH)	824.83 ± 57.56	560.73 ± 40.94	615.50 ± 52.07	249.00 ± 26.67		162.73 ± 22.48	39.41 ± 9.44
s27-LS220							
(NO)	463.55 ± 38.88	536.80 ± 43.79	247.19 ± 27.99	247.63 ± 28.81	93.76 ± 11.30		44.31 ± 8.61
(NH)	369.91 ± 33.40	426.20 ± 37.00	178.54 ± 22.90	171.55 ± 22.55	96.42 ± 11.32		45.05 ± 8.45
(IH)	264.98 ± 27.51	300.79 ± 29.51	113.16 ± 18.12	91.56 ± 15.25	104.05 ± 11.51		50.57 ± 8.65
s27-SFHo							
(NO)	519.96 ± 42.57	426.63 ± 36.68	331.64 ± 34.82	169.21 ± 22.46	53.38 ± 9.54	55.13 ± 11.89	
(NH)	482.12 ± 41.20	359.41 ± 32.40	316.41 ± 34.63	126.58 ± 18.60	46.57 ± 8.98	58.63 ± 12.48	
(IH)	455.17 ± 41.21	278.68 ± 27.54	329.06 ± 36.68	80.04 ± 14.26	34.92 ± 7.87	69.56 ± 13.89	

ACKNOWLEDGMENTS

We thank the Garching group for giving access to their SN neutrino emission models. J.O. is grateful to Ermal

Rrapaj and Andre Sieverding for useful discussions. This work was supported in part by the US Department of Energy under grant DE-FG02-87ER40328. Calculations were carried out with resources of the Minnesota Supercomputing Institute.

-
- [1] H.-T. Janka, Explosion Mechanisms of Core-Collapse Supernovae, *Annu. Rev. Nucl. Part. Sci.* **62**, 407 (2012).
- [2] A. Mirizzi, I. Tamborra, H.-T. Janka, N. Saviano, K. Scholberg, R. Bollig, L. Hudepohl, and S. Chakraborty, Supernova Neutrinos: Production, Oscillations and Detection, *Riv. Nuovo Cim.* **39**, 1 (2016).
- [3] H. Nagakura, A. Burrows, and D. Vartanyan, Supernova neutrino signals based on long-term axisymmetric simulations, *Mon. Not. R. Astron. Soc.* **506**, 1462 (2021).
- [4] J. Olsen and Y.-Z. Qian, Comparison of simulated neutrino emission models with data on Supernova 1987A, *Phys. Rev. D* **104**, 123020 (2021).
- [5] <https://wwwmpa.mpa-garching.mpg.de/ccsnarchive/>.
- [6] K. Hirata *et al.*, Observation of a Neutrino Burst from the Supernova SN1987A, *Phys. Rev. Lett.* **58**, 1490 (1987).
- [7] K. S. Hirata *et al.*, Observation in the Kamiokande-II detector of the neutrino burst from supernova SN1987A, *Phys. Rev. D* **38**, 448 (1988).
- [8] K. Scholberg, Supernova neutrino detection, *Annu. Rev. Nucl. Part. Sci.* **62**, 81 (2012).
- [9] K. Abe *et al.*, Supernova Model Discrimination with Hyper-Kamiokande, *Astrophys. J.* **916**, 15 (2021).
- [10] K. Abe *et al.*, Hyper-Kamiokande Design Report, arXiv:1805.04163 [physics.ins-det] (2018).
- [11] J. Migenda, *Supernova Model Discrimination with Hyper-Kamiokande*, Ph.D. thesis, University of Sheffield (2019).
- [12] T. J. Loredo and D. Q. Lamb, Bayesian analysis of neutrinos observed from supernova SN 1987A, *Phys. Rev. D* **65**, 063002 (2002).
- [13] J. M. Lattimer and D. F. Swesty, A generalized equation of state for hot, dense matter, *Nucl. Phys.* **A535**, 331 (1991).
- [14] A. W. Steiner, M. Hempel, and T. Fischer, Core-collapse supernova equations of state based on neutron star observations, *Astrophys. J.* **774**, 17 (2013).

TABLE VII. The mean Bayes factors along with standard deviations $\langle \ln B_{\alpha\beta} \rangle \pm \sigma[\ln B_{\alpha\beta}]$ calculated for the assumed SK-like detector and an SN at $d = 25$ kpc. The true model M_α can be distinguished from the alternative M_β at the $> 95\%$ CL for $\langle \ln B_{\alpha\beta} \rangle - 1.645\sigma[\ln B_{\alpha\beta}] > 5$, which is satisfied by all the entries.

$M_\alpha \backslash M_\beta$	z9.6-LS220	z9.6-SFHo	s18.6-LS220	s18.6-SFHo	s20-SFHo	s27-LS220	s27-SFHo
z9.6-LS220							
(NO)		27.53 ± 6.55	31.53 ± 7.23	63.84 ± 9.16	391.32 ± 20.00	207.82 ± 15.89	218.92 ± 15.89
(NH)		31.21 ± 6.89	31.64 ± 7.33	64.14 ± 9.08	358.23 ± 19.43	178.84 ± 15.27	202.58 ± 15.36
(IH)		39.94 ± 7.72	33.68 ± 7.62	67.01 ± 9.03	306.16 ± 17.90	135.65 ± 13.75	180.62 ± 14.19
z9.6-SFHo							
(NO)	37.46 ± 10.29		74.85 ± 12.31	44.87 ± 8.53	370.16 ± 20.28	221.95 ± 15.86	199.28 ± 15.93
(NH)	43.40 ± 11.19		85.37 ± 13.38	43.74 ± 8.50	334.21 ± 19.96	194.77 ± 15.52	179.99 ± 15.60
(IH)	56.94 ± 12.98		109.97 ± 15.54	43.11 ± 8.51	273.31 ± 18.91	152.91 ± 14.50	149.65 ± 14.73
s18.6-LS220							
(NO)	38.00 ± 9.57	81.50 ± 13.78		34.87 ± 6.63	269.86 ± 16.75	114.4 ± 12.03	134.10 ± 12.26
(NH)	37.19 ± 9.34	90.23 ± 14.33		40.81 ± 7.19	242.20 ± 15.86	88.97 ± 11.00	123.32 ± 11.58
(IH)	39.01 ± 9.49	112.73 ± 15.89		54.43 ± 8.38	205.12 ± 13.88	56.90 ± 8.91	115.33 ± 10.46
s18.6-SFHo							
(NO)	97.48 ± 17.27	55.14 ± 11.63	55.80 ± 13.36		209.25 ± 16.04	110.04 ± 11.70	84.02 ± 10.74
(NH)	99.96 ± 17.67	52.52 ± 11.23	65.31 ± 14.50		178.11 ± 15.36	86.15 ± 10.98	68.13 ± 10.04
(IH)	109.06 ± 18.82	50.56 ± 10.92	86.65 ± 16.76		129.15 ± 13.65	53.74 ± 9.45	45.99 ± 8.58
s20-SFHo							
(NO)	753.64 ± 53.57	657.68 ± 48.15	523.8 ± 45.21	342.86 ± 33.58		100.98 ± 17.25	46.04 ± 10.40
(NH)	678.53 ± 50.69	549.23 ± 42.18	476.86 ± 43.63	270.00 ± 28.62		106.00 ± 17.83	39.51 ± 9.55
(IH)	598.66 ± 48.67	410.65 ± 34.92	444.43 ± 43.85	181.61 ± 22.69		118.51 ± 19.13	28.89 ± 8.07
s27-LS220							
(NO)	338.28 ± 33.03	390.66 ± 37.03	179.96 ± 23.73	180.02 ± 24.36	68.50 ± 9.66		32.21 ± 7.33
(NH)	270.70 ± 28.47	312.09 ± 31.50	130.17 ± 19.47	125.40 ± 19.18	70.45 ± 9.68		32.84 ± 7.21
(IH)	193.39 ± 23.43	220.54 ± 25.15	81.73 ± 15.33	66.74 ± 12.96	76.02 ± 9.84		36.96 ± 7.39
s27-SFHo							
(NO)	378.39 ± 36.12	311.41 ± 31.16	240.68 ± 29.44	123.41 ± 19.07	39.28 ± 8.19	40.08 ± 10.12	
(NH)	350.88 ± 34.96	263.39 ± 27.65	229.34 ± 29.26	92.61 ± 15.86	34.26 ± 7.71	42.68 ± 10.63	
(IH)	330.26 ± 34.88	204.29 ± 23.52	237.52 ± 30.92	58.31 ± 12.14	25.63 ± 6.75	50.69 ± 11.83	

TABLE VIII. The mean Bayes factors along with standard deviations $\langle \ln B_{\alpha\beta} \rangle \pm \sigma[\ln B_{\alpha\beta}]$ for comparing different scenarios of neutrino oscillations for the same underlying SN neutrino emission model z9.6-LS220. Three SN distances $d = 50, 25,$ and 10 kpc are used and the ideal detector is assumed. The true model M_α can be distinguished from the alternative M_β at the $> 95\%$ CL for $\langle \ln B_{\alpha\beta} \rangle - 1.645\sigma[\ln B_{\alpha\beta}] > 5$, which is satisfied by all the entries except for those in bold.

$M_\alpha \backslash M_\beta$	(NO)	(NH)	(IH)
$d = 50$ kpc			
(NO)		1.10 ± 1.35	7.48 ± 3.44
(NH)	1.37 ± 1.89		3.15 ± 2.38
(IH)	9.98 ± 5.31	3.53 ± 2.82	
$d = 25$ kpc			
(NO)		4.39 ± 2.71	29.92 ± 6.88
(NH)	5.46 ± 3.77		12.60 ± 4.76
(IH)	39.94 ± 10.61	14.11 ± 5.64	
$d = 10$ kpc			
(NO)		27.44 ± 6.77	186.98 ± 17.21
(NH)	34.15 ± 9.43		78.73 ± 11.91
(IH)	249.6 ± 26.53	88.21 ± 14.11	

TABLE IX. The mean Bayes factors along with standard deviations $\langle \ln B_{\alpha\beta} \rangle \pm \sigma[\ln B_{\alpha\beta}]$ for comparing different scenarios of neutrino oscillations for the same underlying SN neutrino emission model s20-SFHo. Three SN distances $d = 50, 25,$ and 10 kpc are used and the ideal detector is assumed. The true model M_α can be distinguished from the alternative M_β at the $> 95\%$ CL for $\langle \ln B_{\alpha\beta} \rangle - 1.645\sigma[\ln B_{\alpha\beta}] > 5$, which is satisfied by all the entries except for those in bold.

$M_\alpha \backslash M_\beta$	(NO)	(NH)	(IH)
$d = 50$ kpc			
(NO)		2.66 ± 2.23	24.49 ± 7.10
(NH)	2.95 ± 2.63		11.18 ± 4.84
(IH)	25.36 ± 7.57	10.82 ± 4.61	
$d = 25$ kpc			
(NO)		10.63 ± 4.46	97.96 ± 14.20
(NH)	11.81 ± 5.25		44.73 ± 9.68
(IH)	101.45 ± 15.14	43.28 ± 9.22	
$d = 10$ kpc			
(NO)		66.41 ± 11.14	612.26 ± 35.49
(NH)	73.83 ± 13.13		279.57 ± 24.20
(IH)	634.05 ± 37.85	270.52 ± 23.06	

- [15] I. Tamborra, B. Mueller, L. Huedepohl, H.-T. Janka, and G. Raffelt, High-resolution supernova neutrino spectra represented by a simple fit, Phys. Rev. D **86** (2012).
[16] W. C. Haxton, Nuclear response of water Cherenkov de-

- tectors to supernova and solar neutrinos, Phys. Rev. D **36**, 2283 (1987).
[17] A. Strumia and F. Vissani, Precise quasielastic neutrino/nucleon cross-section, Phys. Lett. B **564**, 42 (2003).

TABLE X. Values of A_{\min} in units of 10^{29} required to distinguish between the true models (M_α) and the alternatives (M_β) assuming the ideal detector characteristics. Note that $A = 2.14 \times 10^{33} (\text{kpc}/d)^2$ for the ideal detector.

$M_\alpha \backslash M_\beta$	z9.6-LS220	z9.6-SFHo	s18.6-LS220	s18.6-SFHo	s20-SFHo	s27-LS220	s27-SFHo
z9.6-LS220							
(NO)		11.06	55.92	11.68	4.22	7.08	6.04
(NH)		9.64	68.68	10.69	4.40	9.11	6.07
(IH)		7.41	71.60	8.59	4.01	11.24	5.12
z9.6-SFHo							
(NO)	10.60		7.81	37.51	5.51	4.97	8.99
(NH)	9.31		6.90	43.87	7.08	6.22	11.78
(IH)	7.26		5.33	48.58	10.29	8.22	16.79
s18.6-LS220							
(NO)	39.66	5.82		8.63	3.23	6.21	4.50
(NH)	49.08	5.13		7.21	3.26	8.14	4.34
(IH)	51.62	3.93		5.27	2.81	10.17	3.49
s18.6-SFHo							
(NO)	7.60	25.42	7.77		5.27	5.00	9.44
(NH)	7.09	30.48	6.60		6.99	6.83	13.42
(IH)	5.89	35.55	4.97		10.79	11.14	23.01
s20-SFHo							
(NO)	1.45	1.94	1.55	2.73		6.13	26.10
(NH)	1.62	2.65	1.65	3.79		5.66	33.38
(IH)	1.64	4.30	1.57	6.36		4.75	53.55
s27-LS220							
(NO)	3.19	2.27	3.89	3.34	8.15		9.77
(NH)	4.38	3.01	5.43	4.80	7.52		9.48
(IH)	6.08	4.44	7.57	8.59	6.29		8.43
s27-SFHo							
(NO)	2.67	4.07	2.76	6.26	33.64	9.48	
(NH)	2.81	5.58	2.78	9.20	42.43	9.08	
(IH)	2.58	8.64	2.41	16.51	66.23	7.88	

- [18] R. M. Bionta *et al.*, Observation of a neutrino burst in coincidence with Supernova 1987A in the Large Magellanic Cloud, *Phys. Rev. Lett.* **58**, 1494 (1987).
- [19] K. Abe *et al.*, First Gadolinium Loading to Super-Kamiokande, arXiv:2109.00360 [physics.ins-det] (2021).
- [20] A. S. Dighe and A. Y. Smirnov, Identifying the neutrino mass spectrum from a supernova neutrino burst, *Phys. Rev. D* **62**, 033007 (2000).
- [21] M. C. Gonzalez-Garcia, M. Maltoni, and T. Schwetz, Updated fit to three neutrino mixing: Status of leptonic CP violation, *J. High Energy Phys.* **11** (2014) 052.
- [22] P. Zyla *et al.* (Particle Data Group), Review of Particle Physics, *Prog. Theor. Exp. Phys.* (2020), 083C01.
- [23] K. Abe *et al.*, Solar neutrino measurements in Super-Kamiokande-IV, *Phys. Rev. D* **94**, 052010 (2016).
- [24] N. Panagia, R. Gilmozzi, F. Macchetto, H. M. Adorf, and R. P. Kirshner, Properties of the SN 1987A circumstellar ring and the distance to the Large Magellanic Cloud, *Astrophys. J.* **380**, L23 (1991).
- [25] N. Panagia, A Geometric Determination of the Distance to SN 1987A and the LMC, *Springer Proc. Phys.* **99**, 585 (2005).
- [26] R. Barlow, Extended maximum likelihood, *Nucl. Instrum. Methods Phys. Res., Sect. A* **297**, 496 (1990).
- [27] F. D. Schönbrodt and E.-J. Wagenmakers, Bayes factor design analysis: Planning for compelling evidence, *Psychon. Bull. Rev.* **25**, 128 (2018).
- [28] A. M. Stefan, Q. F. Gronau, F. D. Schönbrodt, and E.-J. Wagenmakers, A tutorial on Bayes Factor Design Analysis using an informed prior, *Behav. Res. Methods* **51**, 1042 (2019).

TABLE XI. Values of A_{\min} in units of 10^{29} required to distinguish between the true models (M_α) and the alternatives (M_β) assuming the SK-like detector characteristics. Note that $A = 1.61 \times 10^{33}(\text{kpc}/d)^2$ for the SK-like detector.

$M_\alpha \backslash M_\beta$	z9.6-LS220	z9.6-SFHo	s18.6-LS220	s18.6-SFHo	s20-SFHo	s27-LS220	s27-SFHo
z9.6-LS220							
(NO)		11.40	60.26	12.06	4.52	7.73	6.42
(NH)		9.91	75.74	11.03	4.70	9.98	6.42
(IH)		7.61	82.64	8.86	4.24	12.34	5.38
z9.6-SFHo							
(NO)	11.01		8.27	43.30	6.23	5.52	10.18
(NH)	9.64		7.28	50.90	8.05	6.91	13.48
(IH)	7.51		5.61	56.41	11.85	9.13	19.54
s18.6-LS220							
(NO)	42.44	6.08		8.83	3.40	6.60	4.67
(NH)	53.70	5.34		7.38	3.41	8.63	4.49
(IH)	59.05	4.09		5.40	2.91	10.73	3.59
s18.6-SFHo							
(NO)	7.81	28.94	7.97		5.66	5.31	10.01
(NH)	7.28	35.00	6.77		7.52	7.26	14.28
(IH)	6.06	41.21	5.11		11.69	11.89	24.88
s20-SFHo							
(NO)	1.53	2.13	1.61	2.88		6.27	28.01
(NH)	1.69	2.93	1.71	4.02		5.79	35.79
(IH)	1.71	4.85	1.62	6.82		4.86	57.43
s27-LS220							
(NO)	3.42	2.45	4.09	3.50	8.34		10.04
(NH)	4.72	3.26	5.70	5.04	7.69		9.71
(IH)	6.59	4.83	7.95	9.09	6.43		8.61
s27-SFHo							
(NO)	2.80	4.50	2.85	6.58	36.29	9.78	
(NH)	2.93	6.25	2.86	9.70	45.70	9.34	
(IH)	2.68	9.88	2.47	17.69	71.28	8.07	